Prediction of the elastic modulus of the trabecular bone based on X-ray computed tomography

Kamel Madi, G. Aufort, Alain Gasser, Samuel Forest

Prediction of the elastic modulus of the trabecular bone based on X-ray computed tomography

K. Madi[1], G. Aufort[2], A. Gasser[2], and S. Forest[1]

[1] Centre des Matériaux, Mines ParisTech, Evry, France
[2] Institut Prisme, PolyTech Orléans, Orléans, France

Abstract— **This work aims to estimate the apparent Young's modulus of real human trabecular bones using a numerical micro-macro approach. Cylindrical specimens of trabecular bone were extracted from human femur heads, cleaned and scanned using a SkyScan-1072 micro-computed tomography system. 3D volumetric tetrahedral grids were generated from the exploitation of the reconstructed images using original meshing techniques. Numerical compressive tests were simulated, assuming isotropic tissue Young's modulus for all elements. The large size of the volumes implies grids with a high number of nodes, which required the use of a large number of parallel processors in order to perform the finite element calculations. Numerical Young's moduli varied between 1300 MPa and 1600 MPa, with a good agreement with experiments.**

Keywords— **trabecular bone, Young's modulus, microCT, parallel computing, osteoporosis.**

I. Introduction

The investigation of the mechanical properties of trabecular bone presents a major challenge and could be of great importance to diagnose the bone fracture risk for osteoporosis patients so that preventive measures can be taken in time. Current methods based on bone mineral density measurements or CT techniques are not always predictive of fracture risk or therapy response and might lead to over-diagnosis [1]. Since most osteoporotic bone fractures are initiated in the trabecular bone, several studies have shown that bone strength, an indicator for bone fracture risk, can be better represented by taking into account its complex microstructure.

A promising alternative technique that takes bone microarchitecture into account is microstructural finite element (microFE) analysis. High-resolution images (~10-50-µm resolution) obtained from micro-CT scanning of cancellous bone samples can be digitized and converted to micro-finite element models (FEM) on which compression tests are simulated numerically [2]. A common method to create the finite element meshing from CT images is the voxel-element technique. This method uses the natural discretisation of the image by voxels. Then, each voxel belonging to the solid region constitutes an four-node cubic element of the mesh. A very large number of finite elements are thus needed to accurately represent a human bone with its intricate microarchitecture. Hence, the resulting microFE models possess a very large number of degrees of freedom and require the use of supercomputing [3, 4]. However, this method is often unable to capture surface boundaries satisfactorily (it generates jagged boundaries) which can lead to inaccurate finite element analysis results.

An alternative approach is to create a tetrahedral mesh based on a triangular surface model of the tomographic data [5, 6]. Triangulated surfaces represent the boundaries between the different phases creating a more representative representation of the trabecular bone surface. Even if this method reduces the number of degrees of freedom, parallel computing can be required for large samples and to our knowledge a little has been done on large scale computations using this second approach in the field of biomechanics.

In this work, a 3D complete numerical model of a human femoral head trabecular bone (cylinder of dimensions 12 mm height and 8 mm diameter) was built by combining microCT with finite element modeling using the second method. Sophisticated parallel computing was used to perform the calculations. The objective was to assess the ability of this model to correctly predict the Young's modulus of the trabecular bone. The predicted Young's modulus from compression tests was compared to experimentally determined Young's modulus value.

II. Material and methods

Cylindrical specimens of trabecular bone, of dimensions 12mm height and 8mm diameter, were extracted from freshly harvested healthy human femur heads at Hôspital of Orléans (IPROS, Institut de Prévention et de Recherche sur l'Ostéoporose) in France. Each of the specimens had soft tissues removed. One of them was selected for this study and was scanned using a SkyScan-1072 micro-computed tomography system with a 17.6 microns nominal resolution. The sample was positioned in the scanner such that its longitudinal axis coincided with the longitudinal axis of the scanner. Segmentation of the 3D image was done using the

Amira Software [7]. The method consisted in choosing a threshold, using an histogram of grey levels as a guide. In our case, the choice of the threshold was imposed naturally. Then, the program sets to white all voxels that are located beyond the threshold (bone), and all other voxels of the image to black (voids). The bone volume fraction of the investigated cylinder (12 mm height, 8 mm diameter) was estimated to 20%. Fig. 1 illustrates a 3D representation of a small volume of the bone, extracted from the stack of the segmented images.

After scanning, compressive test was performed at Institut Prisme of Orléans using an Instron 4411 device equipped with a 5 kN load cell, according to the longitudinal direction of the cylinder. Bone cylinder faces were stuck together with resin endcaps. A clip-on extensometer was mounted on the endcaps, as illustrated in figure 2, for which a specific fixture was designed at IPROS for the gripping. A prescribed compressive displacement was applied to the sample at a speed of 0.25 mm/min, at low strains where the material exhibited linear elastic behavior.

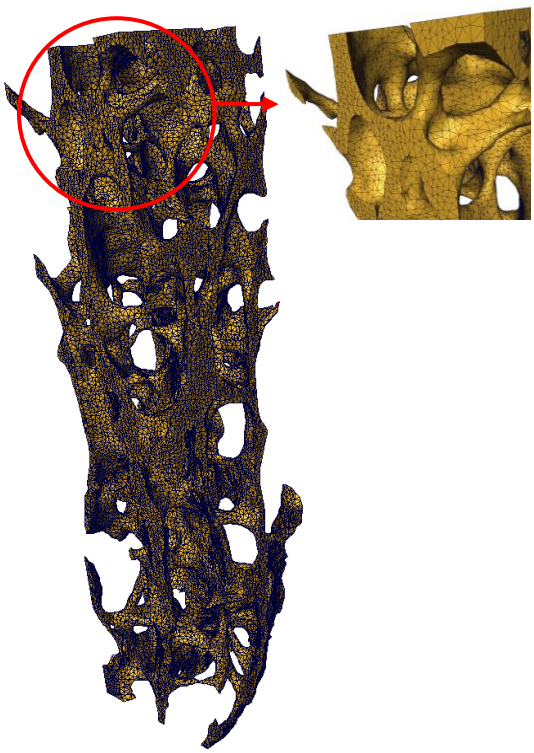

Fig. 1 Three dimensional meshing of a small volume of the trabecular bone, extracted from the cylinder. Dimensions of the volume are 2.2 mm * 2.2 mm * 8.4 mm

III. Computational tools

A. Finite element meshing

Building FE models from 3D voxels requires that the mesh correctly respects the geometry of the phases inside the material. The boundary between the two phases, called the isosurface, has to be well captured before the creation of volumetric grids. In this work, the creation of a surface model with correct topology and optimized triangular shape from the segmented tomographic data is carried out automatically with the help of the marching cubes algorithm [8], using the Amira software. In the last step, an unstructured tetrahedral mesh is built from the basis of the surface triangulation. Here, meshing has been performed using the advancing front method implemented in the Amira software. For the sake of clarity, such 3D grid of the trabecular bone (linear tetrahedral elements) is illustrated in Fig. 1 on a small volume, extracted from the stack of the segmented images. The complete model is depicted in figure 3.

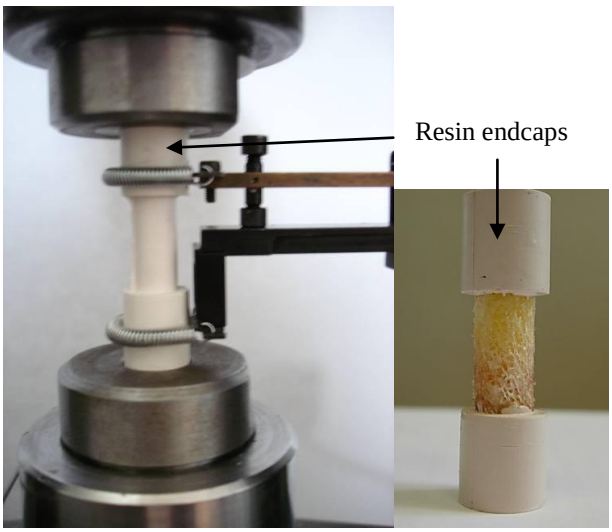

Fig. 2 Experimental device used for compressive tests

B. Elastic properties of the bone

Generally, the mean values of the tissue stiffness are around 15-20 GPa for both cortical and trabecular bone tissue [9, 10, 11]. In this work, the tissue element properties were chosen linear elastic and isotropic with a Young's modulus of 17 GPa and Poisson's ratio of 0.3 [12]. Alternatively, our model could be used to curvefit the value of the tissue stifness such that the numerical apparent Young's modulus value fits the experimental one [13].

C. Parallel computing

The large size of the volumes implies grids with a high number of nodes, which requires the use of a large number of parallel processors in order to perform the finite element calculations. The parallel version of the finite element code ZeBulon is presented in [14, 15]. The problem is solved with the FETI method (Finite Element Tearing and Interconnecting method) [16, 17]. The parallelization scheme is based on a domain decomposition algorithm. The finite element mesh is thus decomposed into several domains. Fig. 3 illustrates the 3D meshing corresponding to the largest computation (complete model containing 1100000 nodes). Each sub-problem is solved independently within a subdomain of the mesh. An additional interface problem is solved. It ensures the compatibility of the displacement between the subdomains. The data exchange between the different tasks uses a PVM communication protocol. In our case, 10 bi-processors (AMD Opteron 248, cadenced at 2.2 Ghz, 8 Go RAM) have been used for a time of calculation less than 20 min.

IV. Results and Discussions

The numerical procedure used to compute the Young's modulus of the trabecular bone is the same that the one used in [18]. Different cylinders having the same diameter (8 mm) with increasing thickness were extracted from the 3D picture and meshed with the same mesh density. One has to notice that when the size of the volume element is smaller than the so-called Representative Volume Element (RVE) of the material, the properties that can be computed are not necessarily the effective properties but merely apparent properties of the investigated volume [19]. The macroscopic Young's modulus obtained after simulating compressive tests according to the longitudinal direction (Oz) was investigated. The (Oz) direction is given by the thickness of the volume. Compressive tests were performed by applying mixed boundary conditions: a displacement is imposed on both faces perpendicular to the (Oz) direction and all the other faces are free of forces. The apparent Young's modulus according to (Oz) direction was determined from the following expression (1):

$$E = \frac{L. < \sigma_{33} >}{\Delta L} f_{vbone} \qquad (1)$$

where, f_{vbone} is the volume fraction of the bone, $< \sigma_{33} >$ is the average stress in the bone according to the (Oz) direction , L is the length of the sample and ΔL is the prescribed displacement. The evolution of the obtained apparent Young's modulus as a function of the volume size is given in Table 1. The calculated Young's moduli were normalised by the one calculated for the largest volume (length of 12mm). Experimental value is also reported.

Table 1 Apparent Young's modulus of the trabecular bone

Thickness of the volume (microns)	1.7	3.5	12
Volume fraction of the bone (%)	16.3	16.6	20
Numerical Young's modulus (GPa)	1490	1380	1537
Relative error (%)	3	10	/
Experimental Young's modulus (GPa)		1224	

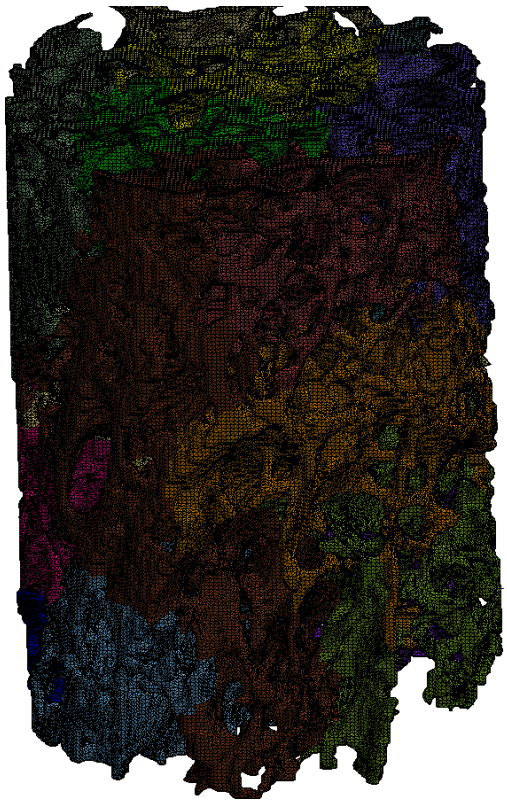

Fig. 3 3D meshing of the trabecular bone cylinder of dimensions 12 mm height and 8 mm diameter. The mesh was built using the method described in section III.A and contains 1100000 nodes (linear tetrahedra). After meshing, the mesh was split into 20 sub-domains for parallel computing

A small bias seems to be observed for smaller volumes where bone volume fractions and Young's moduli are slightly lower than the largest volume. The relative error is less than 10%. Intermediate volumes are under investigation to merely check that the apparent Young's modulus converges towards the value of the largest volume (1537 MPa).

The relative error between the experimental and numerical results is around 11-20%, which seems to be correct when considering only one volume.

V. CONCLUSIONS

This works aims at investigating the accuracy of a 3D numerical model of the trabecular bone based on a multiscale approach. The 3D real bone microstructure was combined with the finite element to predict the Young's modulus of the trabecular bone. The large size of the volumes implied grids with a high number of nodes, which required the use of several processors in order to perform the finite element calculations. Numerical Young's moduli varied between 1300 MPa and 1600 MPa, with reasoneable agreement with experiment. This method is not limited and could be easily applied to more large samples. The model developed in this work will be used later as a reference to validate a new promising beam/shell skeleton-based model [20], in order to provide a low-cost reliable help to early diagnosis of osteoporosis.

ACKNOWLEDGMENT

The authors are grateful to Hôspital of Orléans IPROS (Institut de Prévention et de Recherche sur l'Ostéoporose) in France for providing the bone specimens.

REFERENCES

1. Ahmed AI, Blake GM, Rymer JM, Fogelman I (1997) Screening for osteopenia and osteoporosis: do the accepted normal ranges lead to overdiagnosis? Ost. Int. 7:432-438
2. Hollister SJ, Brennan JM, Kikuchi N (1994) A homogenization sampling procedure for calculating trabecular bone effective stiffness and tissue level stress. *J Biomech* 27:433-444
3. Van Rietbergen B, Weinans H, Huiskes R, Polman BJW (1996) Computational strategies for iterative solutions of large FEM applications employing voxel data. *Int J Numer Meth Eng* 39:2743-2767
4. Bekas C, Curioni A, Arbenz P, Flaig C, van Lenthe GH, Müller R, Wirth AJ (2008) Extreme scalability challenges in micro-finite element simulations of human bone. ISC'08 Proc., International Supercomputing Conference, Dresden, Germany, June 2008, pp 17-20
5. Müller R, Rüegsegger P, (1995) Three-dimensional finite element modelling of non-invasively assessed trabecular bone structures. Med EngPhys 17:126-133
6. Leung SY, Browne M, New AM (2008) Smooth surface micro finite element modelling of a cancellous bone analogue material. Inst Mech Eng H Proc. vol. 222, Jan 2008, pp 145-149
7. Amira. available from: http://wwww.amiravis.com
8. Lorensen WE, Cline H (1987) Marching Cubes: a high resolution 3D surface construction algorithm. SIGGRAPH Proc. Vol. 21, 1987, pp 163–169
9. Cowin SC (2004) Bone Mechanics Handbook. Boca Raton, CRC Press
10. Mente PL, Lewis JL (1987) Young's modulus of trabecular bone tissue. Trans Orthop Res SOC 12:49
11. Young Rho J, Ashman RB, Turner CH (1993) Young's modulus of trabecular and cortical bone material: Ultrasonic and microtensile measurements. JBiom 26: 111-119
12. Bayraktar HH, Morgan EF, Niebur GL, Morris GE, Wong EK and Keaveny TM (2004) Comparison of the elastic and yield properties of human femoral trabecular and cortical bone tissue. JBiom 37:27-35
13. Bevill, G et al (2006) Influence of bone volume fraction and architecture on computed large-deformation failure mechanisms in human trabecular bone. Bone 39: 1218-25.
14. ZSeT/ZeBuLoN (1999). User manual. EMP/LMR/NWNM/ONERA
15. Feyel F, Cailletaud G, Kruch S, Roux, F (1997) Application du calcul parallele aux modeles a grand nombre de variables internes. Colloque national en calcul de structures, Giens, France, 1997
16. Farhat C, Roux FX (1991) A method of finite element tearing and interconnecting and its parallel solution algorithm. Int. J. Numer. Methods. Engrg. **32:**1205–1227
17. Fahrat, C. and Roux, F. (1994) Implicit parallel processing in structural mechanics. Comput. Mech. Adv., 2
18. Madi K, Forest S, Boussuge M, Gailliègue S, Jeulin D, Lataste E, Buffière JY, Bernard D (2006) Finite element simulations of the deformation of fused-cast refractories based on X-Ray computed tomography. CompMatSci 39: 224-229
19. Kanit T, Forest S, Galliet I, Mounoury V, Jeulin D (2003), Determination of the size of the representative volume element for random composites: statistical and numerical approach, Int. J. Solids Struct 40:3647–3679
20. Aufort G, Jennane R, Harba R, Behamou CL (2006), A new 3D shape-dependent skeletonization method. Application to porous media. EUSIPCO, 14th European Signal Processing Conference, Florence, Italy, 2006